50 Years of Spaceflight with Fourier Transform Spectrometers (FTS) built at NASA GSFC

Conor A. Nixon, Shahid Aslam,
John C. Brasunas (Emeritus)
Planetary Systems Laboratory (693)
NASA Goddard Space Flight Center
8800 Greenbelt Road,
Greenbelt, MD 20771
301-286-6757, 301-614-6961
Conor.A.Nixon@nasa.gov
Shahid.Aslam-1@nasa.gov
John.C.Brasunas@nasa.gov

Donald E. Jennings (ret)
Detector Systems Branch (553)
NASA Goddard Space Flight Center
8800 Greenbelt Road,
Greenbelt, MD 20771.
Donald.E.Jennings@nasa.gov

***Abstract*—Over the past 50 years, NASA Goddard Space Flight Center (GSFC) has been developing, building, testing and flying a series of Fourier Transform Spectrometers (FTS). This began with the IRIS instruments on the Earth-orbiting Nimbus satellites and progressed to more sophisticated designs optimized for interplanetary spacecraft sent to Mars and later to the outer solar system. Adaptions have been made over time, including progressively higher spectral resolution, sensitivity, numbers of detectors and complexity. Instrument operating temperatures have decreased to enable remote sensing of the cold giant planet systems. In this paper we describe the historical evolution of this instrument line, comparing and contrasting different aspects such as optical design and materials, detector types and data handling. We conclude by looking towards the future. At present the CIRS-Lite prototype is being tested at NASA GSFC for potential use on a future mission to the ice giants, Uranus and Neptune. Surpassing the previous performance of the Voyager IRIS instruments remains challenging, and new technologies that could enable these measurements are discussed.**

TABLE OF CONTENTS

1. INTRODUCTION

Beginning in the 1960s, a pioneering series of spacecraft-borne Fourier Transform Spectrometers (FTS) have been developed at NASA Goddard Space Flight Center, initiated by the original vision of Rudolf A. Hanel. These were largely based on the Michelson-type of design ([1], Figure 1), where the incoming beam (input port) is split into two equal parts by amplitude, which are then sent down two separate paths before being recombined and sent onwards to a detector (output port). One path (P1) has a fixed retroreflector and hence a fixed path length, while the second (P2) has a moveable retroreflector and therefore a variable path length. By scanning the moveable mirror of the second path, the P2 beam is delayed at positive path difference relative to the fixed path beam P1 (or early at negative path difference), creating interference fringes at the focal plane. The detector samples the time-series of these interference fringes as the mirror is scanned, and the Fourier Transform of the final 'interferogram' is the desired power spectrum of the original signal. This is an idealized description: in practice many complexities are involved, such as the so-called Gibbs phenomenon (or 'ringing', [2, 3]) due to the finite bandwidth of the interferogram, which must be handling by the technique of apodization [4].

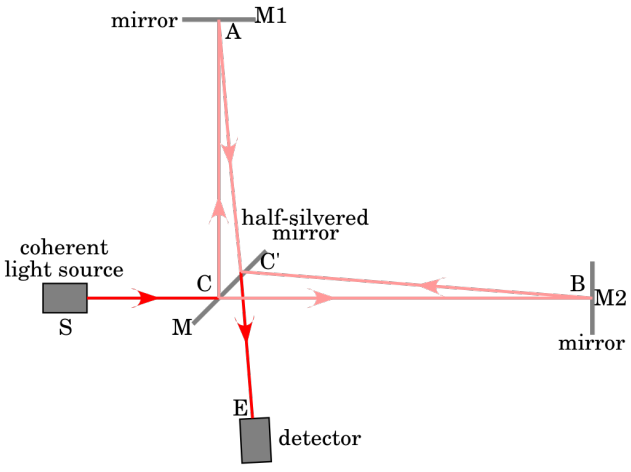

Figure 1: Michelson interferometer optical principle (source: wikipedia commons).

During the 1950s and 1960s interest in Michelson-type interferometers had been revived due to work by Fellgett showing the 'multiplex advantage' of FTS instruments [5] and by Jacquinot and Dufour showing the 'AΩ' or étendue advantage [6]. The multiplex advantage accrues from the fact that the detector at the output port records all frequencies simultaneously, in contrast to a grating spectrometer where each detector only records a discrete frequency at a time. The AΩ advantage relates to the fact that an FTS instrument can have a very high etendue, or optical throughout, relative to other spectrometer types.

Translating this type of instrument to a space environment in the 1960s was highly challenging however, as described in a memorable passage by Hanel [7]:

> *"At the beginning of this project, it was not clear that a wide spectral range, a relatively high resolution, and a high precision could be combined into a small instrument which must also be capable of withstanding the launch and space environment. None of the then-available instruments came close to meeting these requirements, and great doubts existed in the minds of knowledgeable people that such an instrument could be built."*

As the reader may have surmised, the challenges were indeed overcome, and Hanel and colleagues commenced to build a series of successful FTS instruments that have now returned data from planets and moons covering the solar system, from Venus to Neptune. The first was IRIS-A (Infrared Interferometer Spectrometer-A) flown on a high-altitude balloon in 1966. This modest success was a crucial proof-of-concept for remote operation which paved the way for IRIS-B in Earth orbit. The first IRIS-B was lost due to the failure to reach orbit of the Nimbus-B satellite in March 1968. However, the flight spare of IRIS-B on Nimbus 3 in April 1969 was a success, returning data for 3.5 months [7].

IRIS-B was followed by the upgraded IRIS-D on Nimbus-4 in April 1970, with a higher spectral resolution (2.8 cm^{-1} down from 5.0 cm^{-1}) [8]. This instrument also featured an improved telescope, permitting a much better footprint size of 95 km in diameter, reduced from 150 km, and sampling a much more homogeneous area. These were soon followed by IRIS-M, the first interplanetary model, which flew to Mars on Mariner 9 in 1971 [9]. Just as IRIS-B and D had revolutionized our ability to study the Earth atmosphere, IRIS-M provided a similar remote-sensing capability for Mars, a vast improvement compared to Earth-based telescopic observations. Such orders-of-magnitude of increase in information would have been almost unimaginable to the previous generation of scientists, and yet this was only another stepping-stone to the even greater challenge that was to come next: remote sensing of the cold, distant giant planet systems.

Two models of IRIS-V were built: one for each of the Voyager spacecraft that launched in 1977 [10]. IRIS-V had to contend with the much colder temperatures of the outer planetary targets, requiring more drastic changes to the telescope system, detectors and data recording than had occurred in the incremental IRIS-A to IRIS-M progression.

The final flight instrument (so far) in the series of GSFC planetary FTS instrument was another radical improvement and departure from its precursors: the Composite Infrared Spectrometer (CIRS, [11-13]) changed even the name from 'IRIS' to reflect the fact that it was really two inferometers-in-one. These shared the same telescope and foreoptics, but while the now-traditional Michelson design was used for the mid-infrared, a new type of interferometer was implemented for long wavelengths, using the Martin-Puplett principle of beam-splitting by polarization. Moreover, three different detector types - two of them arrays for the first time – were deployed, greatly increasing the overall complexity relative to the IRIS series. This was also the first instrument led by a scientist other than the (then retired) Rudy Hanel: Virgil Kunde oversaw the design and launch of what was to become yet another highly successful spaceflight interferometer-spectrometer. CIRS, part of the Cassini spacecraft payload, went on to map the Saturn system in orbit from 2004-2017.

At the time of writing, a prototype for the next generation instrument is under development: provisionally named 'CIR-Lite' and designed by John Brasunas and colleagues. The focus of the CIRS-Lite design is to reduce size, weight and power relative to CIRS, while retaining high performance and sensitivity, especially for the far-infrared where future applications are envisioned for remote-sensing of the Uranus and Neptune systems.

Table 1 summarizes the parameters and specifications for the Goddard FTS instrument series. In this paper we give an overview of the design evolution of these instruments from IRIS to CIRS and CIRS-Lite, divided into sections on: the telescope and fore-optics; interferometer; reference interferometer; detectors; and read-out and on-board data processing. We conclude by discussing the future possibilities and challenges facing such instrument types in the 21st century.

It is important to mention that none of this work took place in an intellectual vacuum: many other scientists and institutions were simultaneously developing data processing techniques, hardware components and sub-systems, and spacecraft instruments that pioneered various new aspects of the developinng field. Some of these techniques, ideas and even components from 'outside' were incorporated into the Goddard series of instruments, while Goddard itself pioneered in several important areas. In this review article we focus on the major contributions and development on the Goddard side, and encourage the interested reader to seek out a wide variety of review articles and books that can inform as to the wider development of the spacecraft FTS field.

Table 1: Summary of specifications and parameters for GSFC-built spacecraft FTS instruments 1969-2019.

Parameter	**IRIS-B (Nimb. III)**	**IRIS-D (Nimb. IV)**	**IRIS-M (Marin. 9)**	**IRIS V (Voyager)**	**CIRS FP1 (Cassini)**	**CIRS FP3 (Cassini)**	**CIRS FP4 (Cassini)**	**CIRS-Lite (prototype)**
Primary Reference Source	[7][a]	[8][a]	[9][a]	[10][a]	[13][a]			
Launch	14-Apr-69	08-Apr-70	30-May-71	20-Aug-77 05-Sep-77	15-Oct-1997			TBD
Lifetime	3.5 mnths	9 months	17 months	12+ yrs	20 years			N/A
Target(s)	Earth	Earth	Mars	J, S, U, N	Saturn system (flybys of V,E,J)			U, N
Physical								
Mass (kg)	14.5	21.1	25.0	18.4	43.0			18 [b]
Power (W)	16.0	28.0	30.0	14.0	26.4 (32.9)			TBD
Operating Temp. (K)	250	250	250	200	170 ± 0.1			TBD
Blackbody Temp. (K)	280	285	296	N/A	N/A			TBD
Primary Telescope								
Material	Al	Al	Al	Be	Be			[d]
Aperture area (cm^2)	13.0	15.0	15.0	2026.0	2026.0			[d]
Solid angle (sr)	1.57×10^{-3}	5.5×10^{-4}	4.7×10^{-4}	1.7×10^{-5}	1.2×10^{-5} 8.4×10^{-8} 8.4×10^{-8}			[d]
Field of view (°)	8.0	5.0	4.5	0.25	0.22 0.017 0.017			[d]
Focal length [c]	4.1	4.4	4.4	300.0	300.0			[d]
f-number [c]	f/1	f/1	f/1	f/6	f/6			[d]
Interferometer					***FP1***	***FP3***	***FP4***	
Beamsplitter material	KBr	KBr	CsI	CsI	Cu wire grd	KBr	KBr	Diamond
Spectral range (cm^{-1})	400-2000	400-1600	200-2000	180-2500	10-600	600-1100	1100-1500	30-1500
Spectra resol. (cm^{-1}) [e]	5.0 (2.5)	2.8 (1.4)	2.4 (1.2)	4.3 (2.15)	0.5 (0.25)	0.5 (0.25)	0.5 (0.25)	0.25 (0.125)
No. raw samples / IFM	3408	4096	4096	3648	53129	53129	53129	
Ref. wavelength (μm)	0.5852	0.5852	0.6929	0.58525	0.785	0.785	0.785	
Fringes per sample	2	3	1	1	1	1	1	
Max. light path diff. (cm)	0.40	0.72	0.85	0.316	2.08	2.08	2.08	
Mirror velocity ($cm\ s^{-1}$)	0.0184	0.0275	0.0235	0.00351	0.0208	0.0208	0.0208	
IFM duration (s) (max)	10.956	13.107	18.20	45.6	50.0	50.0	50.0	
Frame time (s)	16	16	21	45.6	52.0	52.0	52.0	
Detector(s)					***FP1***	***FP3***	***FP4***	
Type	Si Photod.	Si Photod.			Thermopile	PC HgCdTe	PV HgCdTe	[f]
Operating Temp. (K)	250.0	250.0	250.0	200.0	170.0	77.0	77.0	[f]
Dimensions (mm)	3.0 x 3.0	2.3 x 2.3		2.5 x 2.5	1.0 (circ.)	0.2 x 0.2	0.2 x 0.2	[f]
No, of Detectors	1	1	1	1	1	10	10	[f]
D* ($cm\ Hz^{1/2}\ W^{-1}$)	1.02×10^8	1.02×10^8			4×10^9	2×10^{10}	4.5×10^{11}	[f]
Detector NEP ($W\ Hz^{-1/2}$)			4×10^{-10}	2×10^{-10}	3×10^{-10}	1×10^{-11}	4×10^{-13}	[f]
NESR ($W\ cm^{-2}\ sr^{-1}/cm^{-1}$)	0.6×10^{-7}	0.5×10^{-7}	0.5×10^{-7}	$5\text{-}15 \times 10^{-9}$	4×10^{-9}	4×10^{-9}	3×10^{-10}	[f]
Data								
Onboard reduction factor	-	-	-	-	18	22.5	25.0	TBD
Apodized channels	320	430	750	540	1180	800	1000	TBD
A/D bits	11	11	13	13	12			TBD
Data Rate (bits/s)				1120	4000			TBD

Table notes:

[a] Primary references are sources of all values unless otherwise indicated.

[b] Target value.

[c] Focal length and f-number for the complete optical system.

[d] See discussion in text Section 2.

[e] Numbers in parentheses are unapodized resolution. Maximum resolution is indicated for CIRS, although lower resolutions are allowed.

[f] See text Section 5 for discussion of CIRS-Lite detector options.

2. Telescope and Fore-Optics

The telescope systems may be divided into two main types: the small (~3.5 cm diameter) optical viewing ports of IRIS-B, -D and -M designed for viewing relatively warm targets from low orbits; and the larger (~50 cm diameter) telescopes of IRIS-V and CIRS designed for viewing colder objects from more distant vantage points during flybys. Examples of these are shown in **Figure 2** (IRIS-B) and **Figure 4** (IRIS-V).

Much of IRIS-V (telescope mirrors, interferometer mirrors, housing and support structure) was made of optical grade beryllium, whose low co-efficient of thermal expansion was a key factor in maintaining optical alignment at low temperatures. The primary mirror and reflecting surface in the interferometers were coated with gold over nickel plating [14] to reduce scattering by stray light, a major concern for high phase angle observations made by Voyager, where instruments are pointed close to the Sun to view the dark side of planets and moons. The secondary mirror was coated in aluminum over nickel, and then over-coated with SiO to prevent oxidation. The same telescope system as IRIS-V was used for Cassini CIRS. Note that, behind the large telescopes, the input port to the interferometers remained unchanged from the earlier instruments at ~13 cm^2.

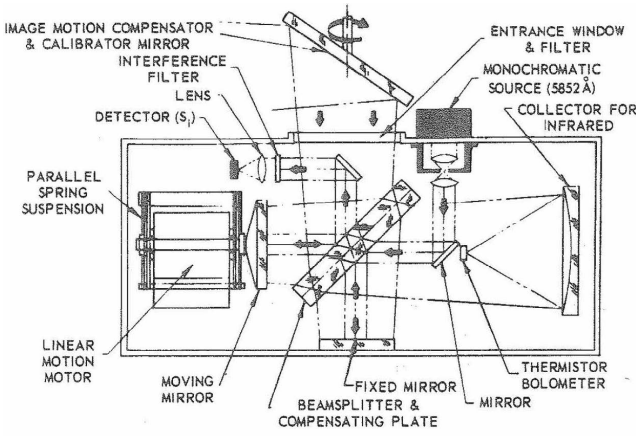

Figure 2: IRIS-B optical layout. The exterior view is selected by rotating the scene-selection mirror at the top through 90-degree steps. The side-look (shown) views the on-board blackbody source, while the upward look (out of page) views deep space for cold calibration target, and the downward view (into page) views the target scene (Earth).

At present, a dedicated telescope system has not been specified for CIRS-Lite. A trade study is planned to assess the primary telescope diameter (dependent on observational strategy) and construction material (Al, SiC or Be). The FTS is currently being evaluated by integrating the FTS to a 1-meter observatory telescope at Goddard.

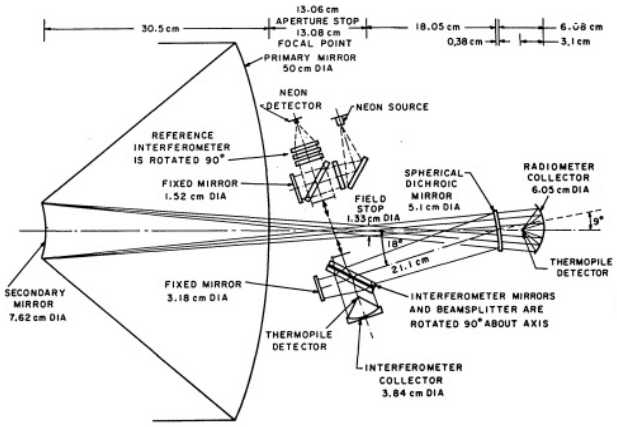

Figure 3: Voyager IRIS optical layout. There is no scene-selection mirror (as with earlier IRIS models) – calibration is achieved by turning to look at deep space for the cold target, and using the internal instrument thermostating to avoid the need for a warm target.

3. Interferometer

IRIS

A major evolution in the interferometer beamsplitter occurred between IRIS-D and IRIS-M, when the previous KBr (potassium bromide) was switched to CsI (cesium iodide), to allow access to longer wavelengths (200-400 cm^{-1}). This was necessary because the Martian atmosphere contains much less water vapor than the Earth's, requiring access to the long-wavelength water spectral lines in the far-infrared for measurement. CsI had previously been rejected as a beamsplitter material for earlier IRIS models due to its difficult mechanical properties, and hygroscopic nature. A ten-layer coating was required for IRIS-M [9], slightly reduced from the 14-layer coating of earlier models.

CIRS

The CIRS instrument was comprised of two separate interferometers (not counting the reference interferometer), although sharing a common set of fore-optics, scan mechanism, reference interferometer and some back-end electronics (**Figure 4**). The incoming beam was divided at a field-splitting mirror into the two interferometers. The mid-IR interferometer was a Michelson type, similar in principle to earlier IRIS models, and returning to a KBr beamsplitter.

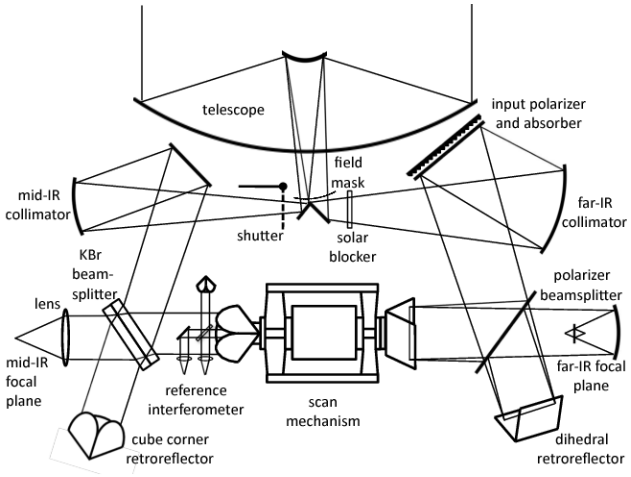

Figure 4: Schematic of the Cassini CIRS optical layout. The incoming beam is divided at a field-splitter (depicted below the telescope secondary) into the two separate interferometers for mid-IR (left) and far-IR (right), described in the text.

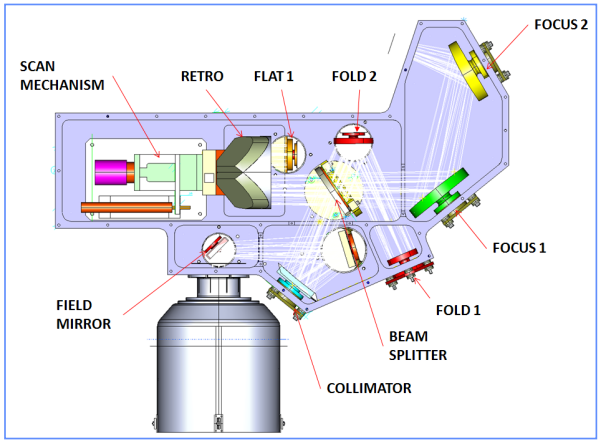

Figure 5: CIRS-Lite optical-mechanical layout, showing the compact design compared to CIRS enabled by the diamond beamsplitter.

The far-IR interferometer, based on the Martin-Puplett design principle [15], was optimized for long wavelengths, and used an input 45° polarizer followed by wire-grid beamsplitter to divide the radiation. The wire-grid beamsplitter was made from 1 μm diameter copper wires placed 2 μm apart on a Mylar substrate [16]. The recombined beam is elliptically polarized and modulated in polarization by movement of the scan mirror. The polarization modulation of the beam is converted back into amplitude modulation by a further 45° polarizer/analyzer placed in front of the detectors, resulting in a conventional interferogram signal.

Both sides of CIRS shared a common scan mechanism, advancing the path difference on one side while reducing it on the other side. This used a similar leaf-spring design to Voyager IRIS, including both mechanical and electromagnetic damping mechanisms.

CIRS-Lite

At present, the CIRS-Lite prototype has focused on the core interferometer section, leaving the telescope and detectors to be selected later depending on specific application. CIRS-Lite aims to reduce the size, weight and power of a next-generation spacecraft FTS compared to CIRS, primarily by achieving broad spectral range coverage in a single-sided system (**Figure 5**). To this end, the beamsplitter has now been replaced with diamond, which has excellent transmission longwards of 5 μm [17]. The flexure carriage mechanism of CIRS was provisionally replaced with a linear mechanism, greatly saving on size and mass.

4. Reference Interferometer

A reference interferometer was an essential component of all the FTS instruments, which generated the closely-spaced fringes used to trigger sampling of the interferogram at uniform intervals. A short wavelength monochromatic source, typically at near-IR wavelengths, is used to create high-frequency interference fringes, and then the sample collection is triggered at some standard multiple of these fringes (every n^{th} fringe).

IRIS-B pioneered the compact optical layout that laid the groundwork for all the successor instruments. A reference neon lamp combined with a narrow-band filter to select a single emission line produced a light source at precisely 0.5852 μm. This was formed into a collimated beam, and then directed into the beamsplitter via a 45° mirror, and onward to the fixed and moveable retroreflectors. After reaching the beamsplitter a second time and recombing, the final, oscillating beam was extracted to a detector (silicon photovoltaic cell) via a second 45° mirror. Sampling was triggered every second fringe. IRIS-D was highly similar but sampled every third fringe to give a longer path length for the mirror motion, and higher spectral resolution. IRIS-M used a similar lamp but filtered on a longer-wavelength neon line (0.6929 μm) and also sampled every third fringe.

For IRIS-V a new approach was used, in which the reference interferometer now had its own entirely separate optics, instead of sharing the optical path with the main beam as in the earlier models. However, the scan mechanism served both the primary interferometer and the reference interferometer, by moving both mirrors attached to opposite ends of the scan carriage. The reference neon wavelengths returned to the original wavelength of 0.5852 μm.

CIRS combined both approaches. The scan mechanism once again served two separate interferometers, moving the variable path retroreflectors of the mid-IR and far-IR interferometers. In this respect it was similar to IRIS-V, but instead of a primary (science) interferometer and reference interferometer, the mechanism served two science interferometers. The third, reference interferometer once again shared optics with a science interferometer, as with

IRIS-B, -D and -M. A 0.785 μm GaAlAs red diode laser was used instead of the neon lamp for longevity and shared the optical path with the mid-IR science interferometer.

CIRS included a second, broadband, 'white-light' LED source at 0.87 μm to provide a reliable zero-path-difference (ZPD) burst (which monochromatic sources do not provide), to enable accurate co-adding of consecutive interferograms.

For CIRS-Lite, the path-sharing approach will once again be used to keep the instrument size and mass as low as possible.

5. DETECTORS

Both IRIS-B and -D used the thermistor bolometers built from silicon photodiodes, although the detector size was reduced from the first to the second to create a smaller field of view. This 5/8 reduction in size, along with the 2x higher spectral resolution of IRIS-D would naturally lead to a higher Noise Equivalent Spectral Radiance (NESR), were it not for other mitigations put in place. These included a reduction in optical path obscuration, a longer scan time, and improvement in the detector bias and pre-amplifier circuit that reduced other sources of electrical noise and allowed IRIS-D to function close to theoretical limits for detector noise.

IRIS-M also used a thermistor bolometer, but a more sensitive photomultiplier type. For IRIS-V, the detector was replaced again, with a Schwartz-type four-element, 18-junction thermopile. The use of a cryogenic detector was considered but rejected due to the long mission duration.

CIRS marked the most radical departure in the use of detectors, splitting the mid and far-infrared interferometers and focal planes. The far-infrared channel (FP1), 17-1000 μm (600-10 cm^{-1}), used two thermocouples similar to the Voyager type, made by the University of Karlsruhe, Germany [18]. These were constructed of gold foil attached to p- and n-doped bismuth telluride posts, with gold-black coating to improve long-wavelength absorption. The two thermopiles were positioned to receive the reflected (FP1R) and transmitted (FP1T) signal from the polarizer-analyzer, and the signals were added in series so as to maximize the signal. Each detector, ~1 mm in diameter, was coupled to the exit port of a parabolic concentrator (sometimes called a 'Winston cone') which had the effect of increasing the collecting area of each by a factor 4. See **Figure 6**.

While the far-IR focal plane (FP1) and detectors operated at the same 170 K temperature as the rest of the instrument, the mid-infrared focal plane (FP3/4) was passively cooled to 75-85 K by use of thermal isolation mounting, and attachment of the focal plane assembly to a radiative cooler 30 cm in diameter that radiated heat directly to space. Thermal stability was ensured by use of small replacement heaters, allowing the temperature to be regulated to ±0.1 K. The 'set point' temperature within this range could be commanded to 22 different settings spaced by 0.4 K, depending on the anticipated heating load. The specific detectivity, D^*, for the FP1 thermopile detector channel is shown in Table 1.

The CIRS mid-infrared focal plane assembly (FPB) is shown in **Figure 7**. A germanium lens focused the beam from the interferometer onto a thermally isolated cold focal plane. Two 1×10 detector arrays recorded the mid-infrared radiation, both identical in dimensions and made from doped HgCdTe material. However, they were each different in detail, and sensitive to different parts of the spectrum. The FP3 array, fabricated at NASA GSFC, operated at longer wavelengths (9-17 μm, 1100-600 cm^{-1}) using the photoconductive (PC) principle. The second array, FP4, built by CEA/Saclay in France, operated at the shortest wavelengths (7-9 μm, 1400-1100 cm^{-1}) and used the photovoltaic (PV) principle. The D^* for FP3 PC and FP4 PV channels are shown in Table 1.

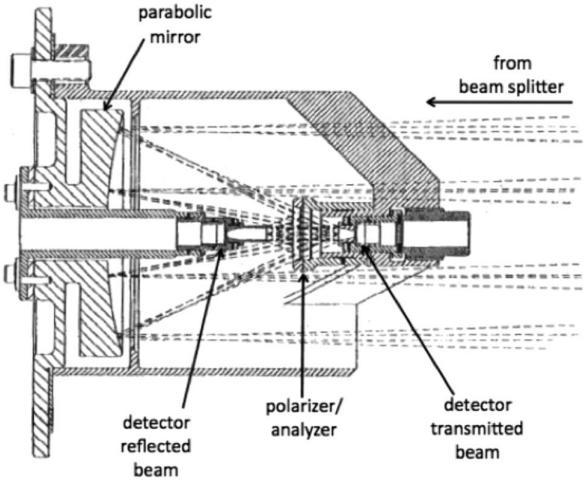

Figure 6: The CIRS far-infrared focal plane assembly (FP1).

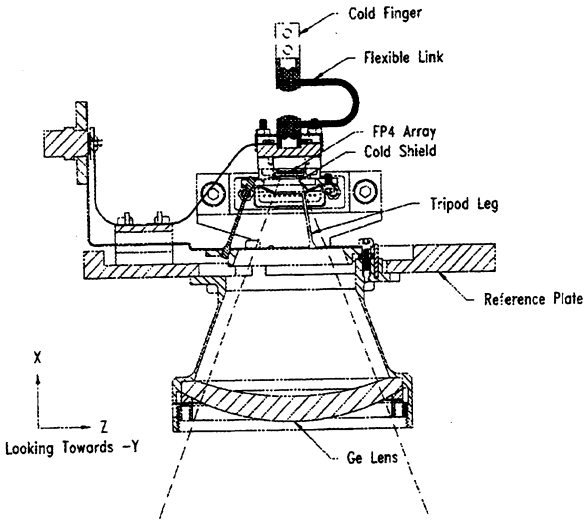

Figure 7: CIRS mid-infrared focal plane assembly (FPB).

Note that several descopes during the Cassini project modified the final CIRS detector arrays from the original proposal: (i) the original mid-IR detector arrays were reduced from 1×20 to 1×10 in length; (ii) the FP2 detector, originally intended to improve sensitivity at 33-17 μm (300-600 cm^{-1}), was removed; (iii) five, rather than ten, read-out channels were assigned to each mid-IR array (FP3 and FP4), meaning that half of the ten detectors could typically be read out at once. This is further examined in the next section.

FIR detectors for CIRS-Lite have not yet been finalized, and will most likely be advanced non-cooled thermopiles, or high transition temperature (high-T_c) superconducting detectors (YBCO and MgB_2), which would require further cooling relative to the CIRS FPB. YBCO thin film high-T_c devices near 89 K were demonstrated in the 1990's, but it was not then possible to construct such devices on substrates amenable to large-array formats with good thermal isolation and high-quality YBCO films. In those days, Si was the obvious substrate candidate, but YBCO film quality was poor. In the 2000's, only small, linear arrays of YBCO could be produced on ultra-thin sapphire substrates (*e.g.* [19-21]). Furthermore, patterning of sub-micron features for circuit elements and interconnects has been difficult due to challenges with etching the ceramic materials. As for read-out electronics, lacking the capability to make features on the sub-ten nm scale has made it difficult to fabricate reproducible Josephson junctions; the basic building block of superconducting electronics for high-T_c bolometer read out.

More recently, fabrication of good quality YBCO thin films on silicon wafers with YSZ/MgO buffer layers with superconducting critical temperature and current density of ~85 K and > 2 MA/cm^2 respectively has been demonstrated in our laboratory with our industrial partners Star Cryoelectronics, iBeam and Ceraco, paving the way for high-temperature superconducting bolometer arrays and superconducting quantum interference device (SQUID) fabrication. Other researchers have demonstrated the operation of a YBCO kinetic-inductance bolometer and have reported a NEP = 3×10^{-13} W/√Hz at 55 K [22]. Single element YBCO bolometers have demonstrated >10 x more sensitivity than the Voyager IRIS and Cassini CIRS thermoelectric detectors.

The superconducting critical temperature (T_c = 39 K) of the simple binary, intermetallic MgB_2 [23] also makes it a very good candidate for the development of the next generation of bolometric devices. In particular, recent advances in deposition techniques to attain high quality polycrystalline MgB_2 thin-film deposited on SiN–Si substrates, with Tc ~38 K [24] together with the observed low voltage noise performance of the film makes it highly desirable for the development of sensitive high-T_c bolometers [25, 26]. A SiN membrane based MgB_2 thin-film bolometer, with a non-optimized absorber, has been fabricated that shows an electrical noise equivalent power of 2.56×10^{-13} W/√Hz operating at 30 Hz [27]. It is therefore important that efforts are made at this stage to mature the MgB_2 thin-film bolometer technology as a potential candidate for integration into a future CIRS-Lite instrument.

If a MgB_2 thin-film bolometer is to be used on future planetary missions, the focal plane assembly will need to be cooled down to 20 K [28], a temperature range not practically attainable with passive radiative coolers. The focal plane will have to be paired with a small mechanical cryocooler with a mass <1 kg, a power consumption of 65 W, operating at a reject temperature of ~170 K (instrument housing temperature). Even though cryocoolers are used on missions such as the Hubble Space Telescope and the James Webb Space Telescope and other missions, there are no space-qualified cryocoolers that presently satisfy the stringent mass and power requirements for outer planet missions. However, substantial efforts are currently underway in both commercial companies, e.g. Sunpower Inc. and Ricor USA Inc. and government agencies, e.g. NASA and DoD, to develop advanced cooling technologies that will meet the requirements to cool MgB_2 bolometer focal plane assemblies and be compatible for outer planet (e.g., Ice Giants) research work [29].

6. Read-out and On-Board Data Processing

The IRIS-B provides a prototype for later read-outs. In order, the steps are:

(1) Pre-amplifier stage: the high-impedance, low noise pre-amp couples with the bolometer to provide flat response across 18-73 Hz.

(2) Numerical filter: the six-pole filter removes signal oustide the active bandpass, with a roll-off of 18 dB/octave.

(3) Gain-changing circuit: the required dynamic range to capture the possible interferogram amplitudes is 1:2000, however the 8-bit analog-to-digital converter (A/D) can capture only 0:127. Therefore, a gain-switching circuit switches the signal from a high to low range with a factor of ten difference before A/D, adding a 0/1 bit for gain type.

(4) 8-bit Analog-to-Digital Converter: the ramp-type A/D is triggers every second fringe of the reference interferometer.

In total, the signal becomes 12 bits: 8 from A/D, 1 gain, 1 parity and 2 synchronization bits.

For IRIS-D, the bias supply and pre-amplifier were changed to lower noise types, and noise was further reduced by moving these to be closer to the detector. Field effect transistors (FETs) were used for both. To capture the higher dynamic range (4000:1) an extra bit was added to the A/D (bringing it to 9), while the gain change factor was reduced from 10 to 4. This simplified later processing, since the high range values were now calculated by a leftward bit shift of 2

positions. The parity bit was removed, keeping the overall bit count at 12. The LSB (least significant bit) magnitude was set to twice the photon (Poisson) noise of the signal, or about 20% of the detector-plus-amplifier noise, meaning that quantization noise did not appreciably affect the output.

For IRIS-M the required dynamic range increased again, to 8000:1, nominally requiring thirteen bits for an A/D without compression. As with IRIS-D, a gain change bit was included, reducing the dynamic range by a factor 4 (2 bits). Secondly, words were co-added in blocks of three, increasing the dynamic range by √3 while reducing the frame count by x3. The LSB of the coadded frame is discarded, saving another 1 bit. The final word length becomes 12 bits: 10 from the A/D, plus 1 for gain switching and 1 for co-adding.

IRIS-V stepped up to a 13-bit A/D, and 14-bit word length after gain-switching by a factor 8 to accommodate the full dynamic range.

Cassini CIRS incorporated similar approaches to previous instruments, including (i) numerical filtering to limit signal bandwidth for each of the three detector types; (ii) down-sampling of raw interferograms (recorded at 1066 Hz) to Nyquist-sampling rate for each of the three focal place band-passes; (iii) encoding and compression with gain-switching, as before; (iv) optional co-adding of interferograms (similar to IRIS-M approach).

7. Conclusions: Future prospects and Challenges

The Goddard-built FTS series of instruments has proved highly successful, advancing in technology during five decades. The FTS-type instrument is particularly powerful in offering a high spectral resolution *and* broad bandpass: an ability that other spectrometer types struggle to match. For example, much higher spectral resolution is available with echelle-etalon type instruments, but these must be tuned to a narrow wavelength range. Similarly gratings must be blazed for a particular wavelength range. However, an FTS in principle can measure an unlimited bandpass simultaneously (in practice, restrictions apply).

Challenge 1: balancing spectral resolution vs SWaP

The relatively high spectral resolution has made the spacecraft FTS instruments especially useful for making atmospheric measurements, where high spectral resolution is required to resolve closely-spaced, over-lapping gaseous emission bands. This has enabled the probing of the chemical composition of the outer planets and Titan, including the detection of new, previously-unseen gases [30-33] and isotopologues [34-38]. However, this ability has come at a cost, with the instruments becoming progressively larger and heavier over time to enable the increased performance. A key challenge going forward will be to once again shrink the size, weight and power (SWaP) – a key objective of the CIRS-Lite development.

Note that the high spectral resolution that is so valuable for atmospheric measurements of narrow lines is much less important for measuring the surfaces of solid bodies, where the spectrum approaches a Planck function, with only slight spectral variation due to mineral content, mainly broad absorption bands (refs). A recent trend in planetary missions to focus on surface geology of mainly airless bodies has led to reduced need and demand for the relatively heavy, expensive and bulky FTS instruments, whose high performance is 'overkill' for those purposes. This situation is likely to change again if a flagship orbiter mission to either Uranus or Neptune (currently under evaluation) is approved, since atmospheric measurements will once again play an important role.

Challenge 2: sensitivity requirements for ice giant missions

A second challenge concerns sensitivity. IRIS-V measurements of Uranus and Neptune had poor S/N of these cold (50-60 K) worlds (Figure 8), which were much more challenging than Jupiter and Saturn. If the proposed Ice Giants Flagship mission does occur, the FTS will need to

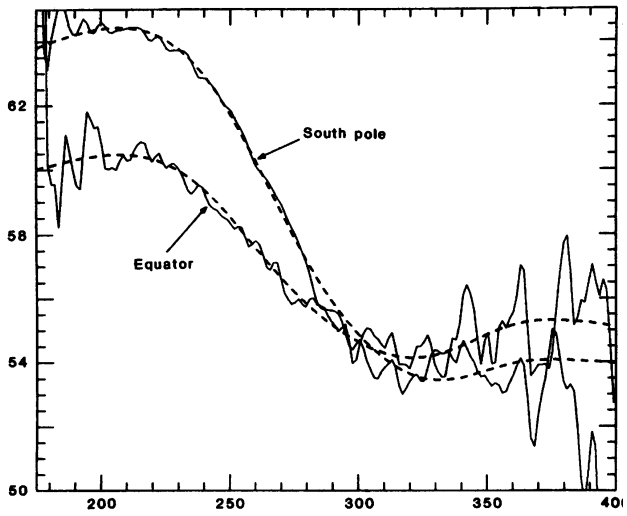

Figure 8: Voyager IRIS brightness temperature spectrum of Uranus, showing the poor S/N away from the Planck function peak towards shorter and longer wavelengths. Only the region from 200-300 cm^{-1} has good S/N.

contend with how to improve S/N relative to IRIS-V, without either a dramatic increase in telescope size, reduction in spectral resolution, or both.

In order to achieve >3-fold improvement in NESR required, for our next generation CIRS-Lite FIR channel (17-1000 μm) we will need higher D^* thermal detectors with highly efficient gold black or impedance matched absorbers and fast thermal time constants. Presently, radiation hard, uncooled thermopiles with $D^* \sim 4\times10^9$ $cmHz^{1/2}/W$ and a time constant of ~30-100 ms are available for spaceflight (*e.g.*, CIRS on Cassini, Diviner on LRO, MERTIS on BepiColumbo). Thermal detectors used for spaceflight instrumentation have consisted of either hand-assembled "one-off" single thermopile pixels (CIRS) or commercial thermopile pixel arrays, both using BiSb(Sb/Te) thermoelectric materials.

Commercially available doped-Si, polysilicon, and VO_x thermopiles have the advantage of being available in large array formats, however, the D^* and time constant performance is only marginally better than the thermal detectors used in CIRS FP1 channel. Progress in the performance of uncooled thermopile detectors will only be made with the discovery of higher Seebeck coefficient materials.

However, thermal detectors based on high-T_c superconducting YBCO and MgB_2 materials already show promise for achieving the required specific detectivity, but the challenges are numerous. The high-T_c detector will need to be operated by a voltage bias at its transition temperature, where its resistance depends very strongly on temperature, this introduces an electrothermal feedback and the current signal is best read out with a sensitive high-T_c SQUID operating at 77 K. These SQUID's have been demonstrated and are actively being worked on and improved in many research laboratories around the world. However, more extensive work has to be done in integrating a high-T_c thermal detector to a high-T_c SQUID readout and demonstrating high performance detection. Typically, the intrinsic noise of a SQUID can be neglected when compared to the thermal detector noise. Additionally, the SQUID current meter has the advantage of low power consumption (nW's). Also, as discussed in §5 the integrated high-T_c thermal detector-SQUID device will require deep cryogenic cooling. The temperature requirements may be achieved by a pulse tube or two stage coolers that have minimum microphonics, but more work has to go into reducing mass, volume and power.

Conclusions

The prospects for remote sensing with FTS instruments remain strong, especially for planetary atmospheres. As well as the potential application to the ice giants, FTS instruments are also excellently suited to study the composition and dynamics of the atmospheres of Saturn, Jupiter, Titan, Mars, Earth and Venus. Further developments in technology, especially super-conducting detectors, will allow FTS' to shrink in size, weight and power requirements, keeping them highly relevant for planetary science applications in the 21st century.

APPENDICES

A. LIST OF ACRONYMS

This is the first appendix. If you have only one appendix, title this section "Appendix."

A/D	Analog to Digital
CIRS	Composite Infrared Spectrometer
DoD	Department of Defence
FET	Field Effect Transistor
FP	Focal Plane
FTS	Fourier Transform Spectrometer
GSFC	Goddard Space Flight Center
IRIS	Infrared Interferometer Spectrometer
LSB	Least Significant Bit
NASA	National Aeronautics and Space Administration
NEP	Noise Equivalent Power
NESR	Noise Equivalent Spectral Radiance
YBCO	Yttrium Barium Copper Oxide
YSZ	Yttrium Stabilized Zirconia

ACKNOWLEDGEMENTS

The authors thank the NASA Cassini Project for partial funding support for the writing of this paper.

REFERENCES

[1] M. A. A., "The Relative Motion of the Earth and the Luminiferous Ether," *Am. J. Sci.,* vol. 22, pp. 120-129, 1881.

[2] H. Wilbraham, "On a certain mathematical function," *The Cambridge and Dublin Mathematical Journal,* vol. 3, pp. 198-201, 1848.

[3] J. W. Gibbs, "Fourier's Series," *Nature,* vol. 59, p. 606, 1899.

[4] F. J. Harris, "On the Use of Windows for Harmonic Analysis with the Discrete Fourier Transform," *Proc. of the IEEE,* vol. 66, no. 1, pp. 51-83, 1978.

[5] P. B. Fellgett, PhD, University of Cambridge, 1951.

[6] P. Jacquinot and C. Dufour, *J. Rech. Centre Nat. Rech. Sci. Lab. Bellevue,* vol. 6, p. 91, 1948.

[7] R. A. Hanel *et al.*, "NIMBUS-III MICHELSON INTERFEROMETER," *Applied Optics,* vol. 9, no. 8, pp. 1767-&, 1970, doi: 10.1364/ao.9.001767.

[8] R. A. Hanel, B. Schlachman, D. Rogers, and D. Vanous, "NIMBUS-4

MICHELSON INTERFEROMETER," *Applied Optics,* vol. 10, no. 6, pp. 1376-+, 1971, doi: 10.1364/ao.10.001376.

[9] R. Hanel *et al.*, "MARINER 9 MICHELSON INTERFEROMETER," *Applied Optics,* vol. 11, no. 11, pp. 2625-+, 1972, doi: 10.1364/ao.11.002625.

[10] R. Hanel *et al.*, "Infrared Spectrometer for Voyager," *Applied Optics,* vol. 19, no. 9, pp. 1391-1400, 1980, doi: 10.1364/ao.19.001391.

[11] V. Kunde *et al.*, *Cassini infrared Fourier spectroscopic investigation* (Cassini/Huygens: a Mission to the Saturnian Systems). 1996, pp. 162-177.

[12] F. Flasar *et al.*, "Exploring the Saturn system in the thermal infrared: The Composite Infrared Spectrometer," *Space Science Reviews,* vol. 115, no. 1-4, pp. 169-297, JAN 2004 2004, doi: 10.1007/s11214-004-1454-9.

[13] D. E. Jennings *et al.*, "Composite infrared spectrometer (CIRS) on Cassini," *Applied Optics,* vol. 56, no. 18, pp. 5274-5294, Jun 2017, doi: 10.1364/ao.56.005274.

[14] J. B. Heaney, L. R. Kauder, S. C. Freese, and M. A. Quijada, "Preferred mirror coatings for uv, visible, and ir space optical instruments," in *Conference on Earth Observing Systems XVII*, San Diego, CA, Aug 13-16 2012, vol. 8510, in Proceedings of SPIE, 2012, doi: 10.1117/12.931005. [Online]. Available: <Go to ISI>://WOS:000326699000014

[15] D. H. Martin and E. Puplett, "POLARISED INTERFEROMETRIC SPECTROMETRY FOR MILLIMETRE AND SUBMILLIMETRE SPECTRUM," *Infrared Physics,* vol. 10, no. 2, pp. 105-&, 1970, doi: 10.1016/0020-0891(70)90006-0.

[16] J. A. Crooke, J. G. Hagopian, K. P. Stewart, S. E. Bradley, and D. Robinson, *Flight qualification of the CASSINI - Composite-InfraRed spectrometer (CIRS) far-infrared (FIR) polarizing beamsplitter substrate: Mylar chosen over polypropylene* (Cryogenic Optical Systems and Instruments Vii). 1996, pp. 128-138.

[17] J. C. Brasunas, G. M. Cushman, and B. Lakew, "Artificial diamond as a broadband infrared beam splitter for Fourier transform spectroscopy," *Applied Optics,* vol. 37, no. 19, pp. 4226-4229, Jul 1998, doi: 10.1364/ao.37.004226.

[18] R. Fettig, B. Lakew, J. Brasunas, J. Crooke, C. Hakun, and J. Orloff, "Thermoelectric infrared detectors with improved mechanical stability for the Composite Infrared Spectrometer (CIRS) far infrared focal plane," in *Cryogenic Optical Systems and Instruments Viii*, vol. 3435, J. B. Heaney and L. G. Burriesci Eds., (Proceedings of the Society of Photo-Optical Instrumentation Engineers (Spie), 1998, pp. 126-135.

[19] J. C. Brasunas and B. Lakew, "HIGH T-C SUPERCONDUCTOR BOLOMETER WITH RECORD PERFORMANCE," *Applied Physics Letters,* vol. 64, no. 6, pp. 777-778, Feb 1994, doi: 10.1063/1.111010.

[20] B. Lakew *et al.*, "High-T-c superconducting bolometer on chemically-etched 7 mu m thick sapphire," *Physica C,* vol. 329, no. 2, pp. 69-74, Jan 2000, doi: 10.1016/s0921-4534(99)00544-4.

[21] B. Lakew, J. C. Brasunas, S. Aslam, and D. E. Pugel, "High-T-c, transition-edge superconducting (TES) bolometer on a monolithic sapphire membrane - construction and performance," *Sensors and Actuators a-Physical,* vol. 114, no. 1, pp. 36-40, Aug 2004, doi: 10.1016/j.sna.2004.02.039.

[22] A. Chakrabarty, M. A. Lindeman, B. Bumble, A. W. Kleinsasser, W. A. Holmes, and D. Cunnane, "Operation of YBCO kinetic-inductance bolometers for outer solar system missions," *Applied Physics Letters,* vol. 114, no. 13, Apr 2019, Art no. 132601, doi: 10.1063/1.5089143.

[23] J. Nagamatsu, N. Nakagawa, T. Muranaka, Y. Zenitani, and J. Akimitsu, "Superconductivity at 39 K in magnesium diboride," *Nature,* vol. 410, no. 6824, pp. 63-64, Mar 2001, doi: 10.1038/35065039.

[24] B. H. Moeckley, K. E. Kihlstrom, A. T. Findikoglu, and D. E. Oates, "Microwave

properties of MgB_2 thin films by reactive evaporation," *IEEE Trans. Appl. Supercon.,* vol. 15, pp. 3308–3312, 2005.

[25] B. Lakew, S. Aslam, H. Jones, B. Moeckly, J. Brasunas, and D. Franz, "Effect of ionizing radiation on noise in MgB2 thin film - a candidate material for detector development for post-Cassini planetary missions," *Physica C-Superconductivity and Its Applications,* vol. 440, no. 1-2, pp. 1-5, Jul 2006, doi: 10.1016/j.physc.2006.03.043.

[26] B. Lakew, S. Aslam, H. Jones, T. Stevenson, and N. Cao, "1/f Noise in the superconducting transition of a MgB2 thin film," *Physica C-Superconductivity and Its Applications,* vol. 470, no. 9-10, pp. 451-455, May 2010, doi: 10.1016/j.physc.2010.03.009.

[27] B. Lakew *et al.*, "MgB2 thin-film bolometer for applications in far-infrared instruments on future planetary missions," *Physica C-Superconductivity and Its Applications,* vol. 483, pp. 119-126, Dec 2012, doi: 10.1016/j.physc.2012.08.007.

[28] A. P. Richards, "Superconducting TES bolometers above 1 K," presented at the International Thermal Detectors Workshop, 2003.

[29] O. Mousis *et al.*, "Scientific rationale for Uranus and Neptune in situ explorations," *Planetary and Space Science,* vol. 155, pp. 12-40, Jun 2018, doi: 10.1016/j.pss.2017.10.005.

[30] V. G. Kunde, A. C. Aikin, R. A. Hanel, D. E. Jennings, W. C. Maguire, and R. E. Samuelson, "C4H2, HC3N AND C2N2 IN TITANS ATMOSPHERE," *Nature,* vol. 292, no. 5825, pp. 686-688, 1981, doi: 10.1038/292686a0.

[31] W. C. Maguire, R. A. Hanel, D. E. Jennings, V. G. Kunde, and R. E. Samuelson, "C3H8 AND C3H4 IN TITANS ATMOSPHERE," *Nature,* vol. 292, no. 5825, pp. 683-686, 1981, doi: 10.1038/292683a0.

[32] R. E. Samuelson *et al.*, "CO2 On Titan," *Journal of Geophysical Research-Space Physics,* vol. 88, no. NA11, pp. 8709-8715, 1983, doi: 10.1029/JA088iA11p08709.

[33] C. A. Nixon *et al.*, "DETECTION OF PROPENE IN TITAN'S STRATOSPHERE," *Astrophysical Journal Letters,* vol. 776, no. 1, Oct 2013, Art no. L14, doi: 10.1088/2041-8205/776/1/l14.

[34] A. Jolly, A. Fayt, Y. Benilan, D. Jacquemart, C. A. Nixon, and D. E. Jennings, "THE nu(8) BENDING MODE OF DIACETYLENE: FROM LABORATORY SPECTROSCOPY TO THE DETECTION OF (13)C ISOTOPOLOGUES IN TITAN'S ATMOSPHERE," *Astrophysical Journal,* vol. 714, no. 1, pp. 852-859, MAY 1 2010 2010, doi: 10.1088/0004-637X/714/1/852.

[35] D. E. Jennings *et al.*, "Isotopic ratios in Titan's atmosphere from Cassini CIRS limb sounding: HC3N in the north," *Astrophysical Journal Letters,* vol. 681, no. 2, pp. L109-L111, Jul 2008, doi: 10.1086/590534.

[36] C. A. Nixon *et al.*, "Isotopic ratios in Titan's atmosphere from Cassini CIRS limb sounding: CO2 at low and midlatitudes," *Astrophysical Journal Letters,* vol. 681, no. 2, pp. L101-L103, Jul 2008, doi: 10.1086/590553.

[37] S. VINATIER, B. BEZARD, and C. NIXON, "The Titan N-14/N-15 and C-12/C-13 isotopic ratios in HCN from Cassini/CIRS," *ICARUS,* vol. 191, no. 2, pp. 712-721, 2007 2007, doi: 10.1016/j.icarus.2007.06.001.

[38] B. Bezard, C. A. Nixon, I. Kleiner, and D. E. Jennings, "Detection of (CH3D)-C-13 on Titan," *Icarus,* vol. 191, no. 1, pp. 397-400, Nov 2007, doi: 10.1016/j.icarus.2007.06.004.

BIOGRAPHY

Conor Nixon *is a scientist in the Planetary Systems Laboratory at NASA Goddard Space Flight Center in Greenbelt, MD. He has 20 years of experience in planetary science research, especially focusing on remote sensing of the atmospheres of the outer*

planets and Titan from spacecraft platforms such as Galileo and Cassini. He was the Deputy Principal Investigator of Cassini's Composite Infrared Spectrometer (CIRS) and has led mission design studies for future missions to Jupiter and Titan. He is currently engaged in instrument development for future planetary missions to the outer solar system, including next-generation infrared FTS instruments.

***Shahid Aslam** is currently employed as a Space Scientist in the Planetary Systems Laboratory, NASA, Goddard Space Flight Center. He received a D.Phil. (Oxon) in Planetary Physics from the University of Oxford, UK in 2006. He has significant instrument hardware development experience with direct contributions to the following NASA flight programs: Pressure Modulated Infra-Red Radiometer (PMIRR) on Mars Observer; Composite Infra-Red Spectrometer (CIRS) on Cassini; Gas and Aerosol Monitoring Sensor-craft (GAMS); Stratospheric Aerosol and Gas Experiment III (SAGE III) and James Web Space Telescope (JWST).*

***John Brasunas** is an emeritus scientist in the Planetary Systems Laboratory at NASA GSFC. Since 1984, he has concentrated on the development and operation of Fourier transform spectrometers (FTS) for the study of planetary atmospheres via passive, infrared remote-sensing for understanding temperatures, winds, and the types of gasses present (including isotopes); ensuring the characterization of global climate systems. He has served on many instrument teams including balloon-borne/ground-based spectroscopic observations of Earth atmosphere with the SIRIS FTS, spectroscopic studies of the Jovian and Saturnian systems with the Cassini CIRS FTS aboard the Cassini orbiter, development of high temperature superconductor (HTS) bolometers needing only moderate cooling and the development of a smaller, lighter FTS known as CIRS-lite.*

***Don Jennings** is an aerospace engineer and scientist at Goddard Space Flight Center in the Detector Systems Branch. His specialty is infrared spectroscopy of atmospheres. During a 41-year career he has served on instrument teams on a variety of Planetary and Earth Science missions, including Cassini, New Horizons, OSIRIS-REx, Earth Observing Mission -1 (EO-1), and the Compact Thermal Imager (CTI) on the International Space Station. His interests have also led to investigations of the infrared solar polarimetry, stellar atmospheric composition, and spacecraft infrared glow (on the Space Shuttle).*